IOP Conf. Series: Journal of Physics: Conf. Series **782** (2017) 012010 doi:10.1088/1742-6596/782/1/012010

On the relation between friction losses and pressure pulsations caused byRotor Stator interaction on the Francis-99 turbine

Petter T.K.Østby[1,2], Jan Tore Billdal[2], Bjørn Haugen[1], Ole Gunnar Dahlhaug[1]

[1]Norwegian University of Science and Technology, Trondheim, Norway
[2]Rainpower Norge AS, Norway

E-mail: petter.oestby@rainpower.no

Abstract. High head Francis runners are subject to pressure pulsations caused by rotor stator interaction. To ensure safe operation of such turbines, it is important to be able to predict these pulsations. For turbine manufacturers it is often a dilemma whether to perform very advanced and time consuming CFD calculations or to rely on simpler calculations to save development time. This paper tries to evaluate simplifications of the CFD model while still capturing the RSI phenomena and ensuring that the calculation does not underpredict the pressure amplitudes. The effects which turbulence modeling, wall friction, viscosity and mesh have on the pressure amplitudes will be investigated along with time savings with each simplification. The hypothesis is that rotor stator interaction is manly driven by inviscid flow and can therefore be modeled by the Euler equations.

1. Introduction

The ability to correctly predict the pressure pulsation due to rotor stator interaction (RSI) in high head Francis turbines has been the subject to research for a long time and the current state of the art methods have good correlation with experimental data [6]. However, when designing new turbines it is often desirable to quickly evaluate effects such as RSI without having to use advanced and time consuming methods. It is also desirable for the quick method to produce conservative results that do not underestimate the pressure pulsations. This paper evaluates the possibility to solve the flow equations without turbulence models and viscosity, in practice the Euler equations, while still modeling the underlying physics of RSI in a low specific speed Francis turbine. This is done by investigating the relation between friction losses in the guide vane domain and pressure pulsations observed in the runner caused by RSI.

The usage of the inviscid Euler equations to predict rotor stator interaction has been common in the aerospace field for decades. In in 1988, Giles [5] presented a numerical analysis of rotor-stator interaction in a low-speed gas turbine. For water turbines, the Euler equations have been used to predict stationary performance since the early 1990s[4, 6], but not for unsteady calculations. It is still common to use in-house Euler solvers to quickly evaluate design changes in a preliminary design phase.

1.1. Euler equations

The Euler equations (1) are a set of equations describing inviscid fluid flow and can be seen as a special case of the Navier-Stokes equations (2) with zero viscosity. Even though the Euler equations can be used for compressible calculations this paper refers only to the incompressible variant.

$$\frac{D\vec{v}}{Dt} = -\frac{\nabla p}{\rho} + \mu\frac{\cancelto{0}{\nabla^2\vec{v}}}{\rho} \tag{1}$$

$$\frac{D\vec{v}}{Dt} = -\frac{\nabla p}{\rho} + \mu\frac{\nabla^2\vec{v}}{\rho} \tag{2}$$

2. Analytical evaluation

The pressure pulsations due to RSI in the runner are, neglecting all acoustic effects, due to the spatially varying pressure field created by the guide vanes. As the guide vanes are obstructions in the flow field, their presence will cause variation in the pressure field. The magnitude of the amplitudes of the pressure field can, disregarding any turbulent and viscous effects, be assumed to be proportional to the velocity squared.

Ignoring the guide vanes for now one can evaluate the domain in which the guide vanes are located as a ring, figure 1, where the water enters at the greater radius and leaves at the smaller. In high head Francis turbines the velocity of the water entering the guide vane domain is often highly tangential. Ignoring friction, the flow can be described using the conservation of spin and conservation of mass which would imply a constant flow angle,α.

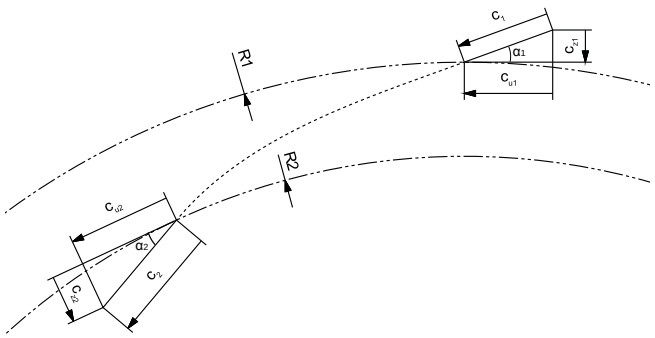

Figure 1. Velocity diagram through circular ring

$$c_u \cdot r = constant \tag{3}$$
$$c_z \cdot r = constant \tag{4}$$
$$\alpha \quad = arctan(\frac{c_z}{c_u}) \tag{5}$$

However, including friction losses in this setup and applying conservation of torque(6) on the boundaries one can show that frictional losses in the tangential direction has to reduce the circumferential velocity, c_u.

$$\int_A (\vec{r} \times \vec{v} \cdot \rho) \cdot (\vec{v} \cdot \vec{n}) dA = \int_A (\vec{r} \times \vec{t}) dA \tag{6}$$

The inlet and outlet boundaries have a radial normal vector and the covers which cause friction have a normal vector in the axial direction. This, together with the assumption that the velocities are constant on the boundaries, equation (6) simplifies to (7), where M is the integral of tangential component of the friction force multiplied by its radius.

$$\dot{m} \cdot (r_1 \cdot c_{u1} - r_2 \cdot c_{u2}) = M \tag{7}$$
$$c_{u2} \quad = c_{u1} \cdot \frac{r_1}{r_2} - \frac{M}{\dot{m} \cdot r_2} \tag{8}$$

Since the velocity of a high head Francis has a large tangential component in the guide vane domain, and thus a large M, the change in friction losses through the guide vane domain is expected to heavily influence the total velocity and thus the spatially varying pressure field. This suggests that a simplified calculation with less friction losses would be a conservative calculation with regards to pressure pulsations due to RSI.

The guide vanes can be included in such an analysis by assuming they behave like hydrofoils in a cascade with lift and drag. The drag will have the same effect as the friction in equation (6) reducing the circumferential velocity. Assuming that the guide vanes have a typical design then the lift will increase the circumferential velocity. Figure 2 shows a schematic representation of how the lift and drag affects the water. Since the lift coefficient is more or less independent of the viscosity and roughness while the drag coefficient is increased with viscosity and roughness [1], one can expect the presence of guide vanes to further enhance the effect fiction has on the circumferential velocity. An increase in friction with or without guide vanes will reduce the circumferential velocity and thus the spatially varying pressure field downstream.

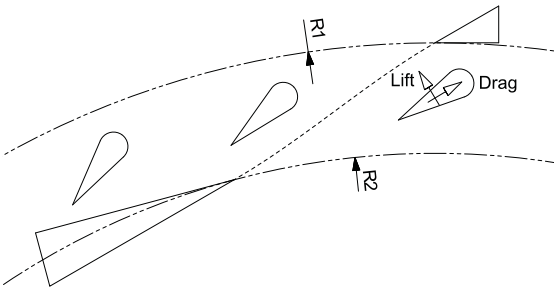

Figure 2. Velocity through circular ring with guide vanes

3. Reference case

The geometries used in this article are based on those provided with the Francis 99 workshop. The turbine is a low specific speed Francis turbine with 14 stay vanes, 28 guide vanes and a runner with 15 full vanes and 15 splitter vanes. The main parameters of the model turbine are given in table 1. Both the runner and the stationary components are equipped with pressure sensors which provide both steady and unsteady measurements. Only the on-board pressure sensors in the runner hub are used in this article. Their locations are shown in figure 3.

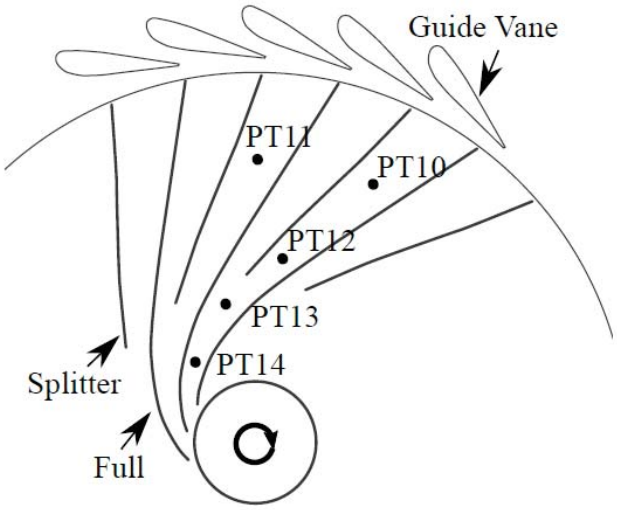

Figure 3. Runner Pressure Sensor Locations [2]

Table 1. Operating parameters of the model at best efficiency point [7]

Parameter	Symbol	Value	Unit
Head	H	12	m
Discharge	Q	0.2	$m^3 s^{-1}$
Power	P	0.022	MW
Runner diameter	d	0.349	m
Runner speed	n	332	rpm
Reynolds number	Re	1.8×10^6	-

4. CFD evaluation

To verify the results from the analytical evaluation two tests were conducted with CFD. First a steady state simulation with only two guide vanes was run. Next a unsteady simulation was performed with the complete runner and all guide vanes. The simulations were performed with Ansys CFX v17.0 and the meshes were generated with Numeca's Autogrid. Different parameters were varied to investigate the relationship between friction losses and pressure pulsations. These changes also affect other parameters such as head, torque and efficiency of the turbine, but these effects are not reported as they are not the subject of this paper.

With the viscosity reduced to zero the system of equations effectively become the Euler equations. Ansys CFX can only solve the Navier-Stokes equations. There is no option to only solve the Euler equations. This means that even with a viscosity of zero the solver still solves the diffusion terms. For the viscous solutions the standard two equation k-ϵ turbulence model is used. The inviscid flow was modeled with turbulence modeling turned off.

4.1. Only guide vanes

4.1.1. Setup A set of simple CFD calculations were conducted including the guide vanes from the Francis-99 test. The setup included two guide vanesat the BEP opening. At the inlet a total pressure condition was used and a mass flow condition was used on the outlet. These conditions were chosen to avoid forcing a pressure field on either of the boundaries. The mass flow was chosen equal to the measured mass flow in the test rig at BEP. The mesh was an all hex mesh with 122880 elements and an average Y+30 with a dynamic viscocity of 10^{-3}.

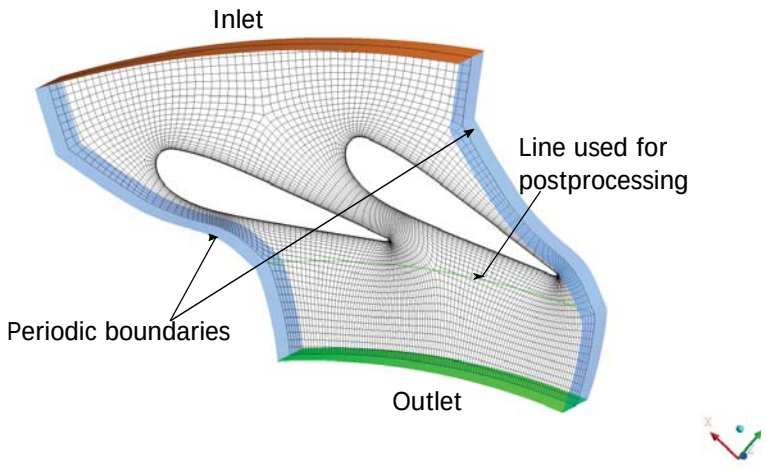

Figure 4. CFD setup for guide vane simulation

The base case was calculated with water, the $k-\epsilon$ turbulence model and hydraulicaly smooth walls with no-slip condition. Later this setup was modified to evaluate the relation between friction losses and pressure variations. All pressure variations are reported as the pressure amplitude at a line located at radius 319 mm, 10mm downstream of the guide vane trailing edge, which is shown in figure 4. Five different parameters were varied one at a time of the base case. The varied parameters are shown in table 2.

Table 2. Varied parameters for the guide vane tests

Parameter	Unit	Values
Main Models	[-]	k-ϵ,SST,laminar,slip/no-slip
Mesh	[# elements]	122880,288000,554240,858880
Dynamic Viscosity	$[\frac{kg}{m\,s}]$	$10^{-2}, 10^{-3}, 10^{-4}, 10^{-6}, 10^{-10}$
Wall Roughness	$[\mu m]$	1,6,12,24,48,100,200,400
Inlet flow angle	[]	15,20,25,30,35,40

4.1.2. Results The results show a clear relationship between the pressure amplitude and circumferential velocity, and also the pressure amplitude and the loss through the guide vane cascade. This is shown in figure 5.

The calculated pressure amplitudes depend mainly on parameters which also affects the circumferential velocity. This is in accordance with the findings of Antonsen [3], even though he reported less differences than what was found here. Changes in mesh and changes in inlet flow angle does not seem to affect neither the velocity nor the pressure amplitudes.

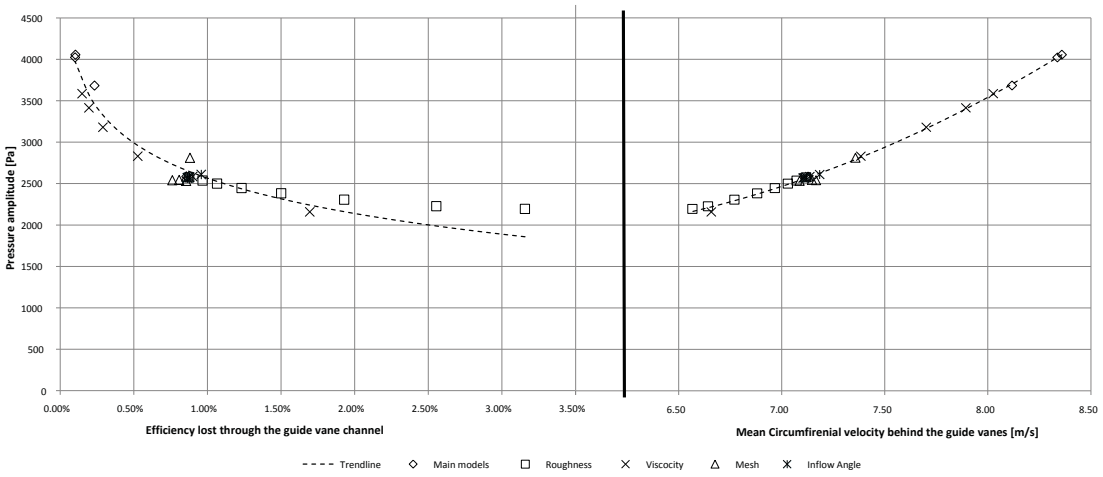

Figure 5. Spatially varying pressure amplitudes behind the guide vanes plotted against (right) local velocity and (left) efficiency lost

4.2. Runner and guide vanes

4.2.1. Setup The effect of the changes in amplitude for the spatially varying pressure field in the runner was evaluated using a full 360 unsteady calculation including both guide vanes and the runner. Three operating points were used in the calculations which are the same as the ones used in the experimental setup. The inlet boundary condition was set to a constant mass flow according to table 3, while the outlet had an average

pressure constraint. Between the runner and guide vane domains a sliding rotor-stator interface was used. The total mesh contained 11.5 mio hex elements and the average Y+ values were 13 in the guide vane domain and 7 in the runner domain using regular water. 30 time steps were used per guide vane passing which equals 0.428 degrees per time step. CFX was required to achieve RMS-residuals of less than 10^{-5} before moving to the next time step. The number of iterations per time step was limited to maximum of 10.

As the variation in viscosity had the greatest impact on the results in the calculations with the guide vanes only, it was chosen as the main parameter to vary in the runner guide vane setup. The dynamic viscosity was varied with the following values $10^{-6}, 10^{-4}, 10^{-3}, 10^{-2}, 0[\frac{kg}{m\,s}]$. When the viscosity was set to zero, no turbulence model was used and slip conditions were applied to all walls. This is similar to using the Euler equations.

The same mesh is used for all values of viscosity. This was done to ensure that any changes in the pressure pulsations are the result of changes in viscosity. At the same time this may introduce an error as the boundary layer will be resolved differently due to Y+ changing with viscosity. The effect of the boundary layers are assumed to be minimal as the flow, especially near BEP, is without separations and recirculation and the automatic wall treatment of the CFX solver can handle large variations in y+.

Table 3. Operating points [2]

		PL	BEP	HL
Guide vane opening	[]	7.00	10.20	12.67
Mass Flow	[kg/s]	139.6	199.6	242.4
Rotational Speed	[rpm]	332.6	332.6	332.6

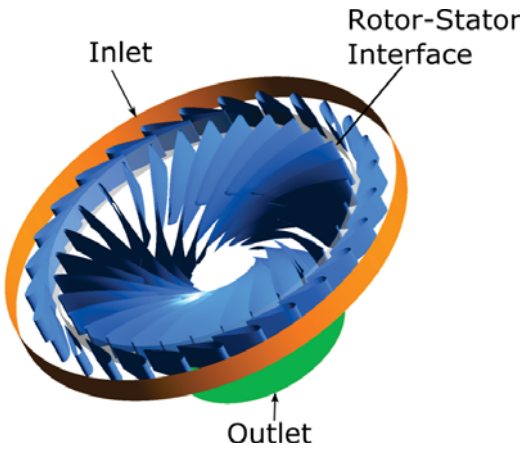

Figure 6. Runner and guide vane domain

4.2.2. Verification To ensure that a proper numerical setup was used, the calculated pressure amplitudes were compared to the measured pressure amplitudes provided by the pressure sensors in the runner hub. Both the phase shift of the time signal and amplitudes between the different sensors are compared to the CFD results. The time signal of the measured values is filtered through a band pass filter of 155 ± 5Hz. The

mean and the 2.5 and 97.5 percentile values are used in the comparison. From the CFD a Fourier series at the guide vane passing frequency is run over the time signal to get the pressure amplitude and phase angle. CFD values are shown with uncertainty bands made from the 2.5 and 97.5 percentile of the values from all runner channels. Figure 8 shows that the phase angles corresponds with the measured values at the inlet but deviates a bit near the outlet. The pressure amplitudes at guide vane passing frequency are shown in figure 7. The pressure amplitudes are over estimated, on average, by 15% in the viscous CFD for all sensor locations. The best agreement between the viscous calculation and measurements is achieved at BEP (11%) while the results at PL (17%) and HL (21%) deviate more.

The calculation is very sensitive to guide vane opening as changes in guide vane opening at a given turbine discharge directly affects the circumferential velocity which again affects the pressure field.

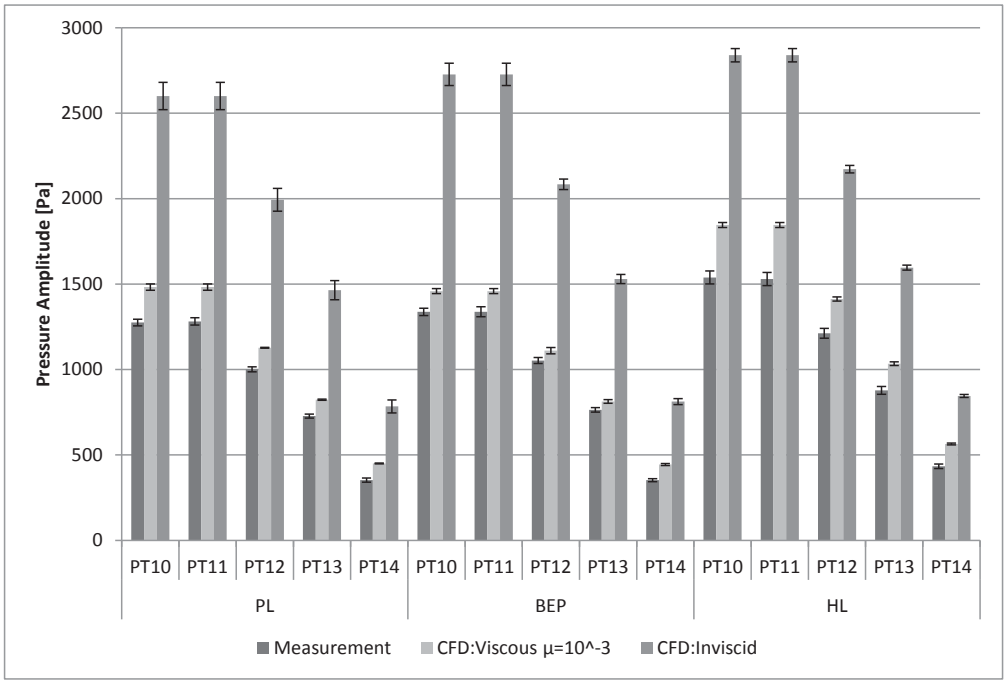

Figure 7. Comparison of measured and calculated pressure amplitudes

4.2.3. Results For each combination of operating point and dynamic viscosity one CFD calculation was run. The calculation runs until a steady and periodic solution is achieved. Then two more guide vane passings are simulated and a Fourier series is used on the pressure field in both the runner and guide vane domains. This extracts the amplitude and phase angle of the pressure field at the first harmonics of the guide vane passing frequency.

The instantaneous pressure field between the runner and guide vanes is shown at the High Load operating point in figure 10 plotted against the tangential position. It clearly shows the increase of the pressure variations with the inviscid solution while the general shape of the pressure field is more or less the same. It also clearly shows that the nodal diameter of the pressure field is ND2, which is visible as the pressure variation with two periods around the circumference. Both the blade passing frequency and the nodal diameter is predicted with the viscous and inviscid method.

How the pressure pulsations in the runner change with viscosity is shown in figure 9. Here the results are reported as the root mean square of the pressure amplitudes in the runner domain at the guide vane

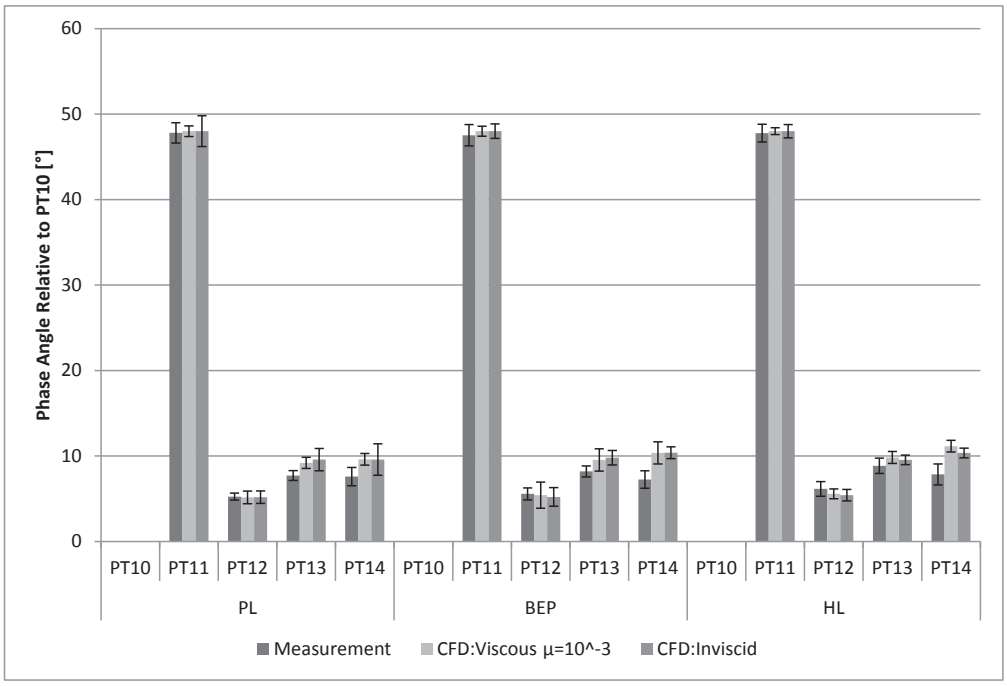

Figure 8. Comparison of measured and calculated phase angles

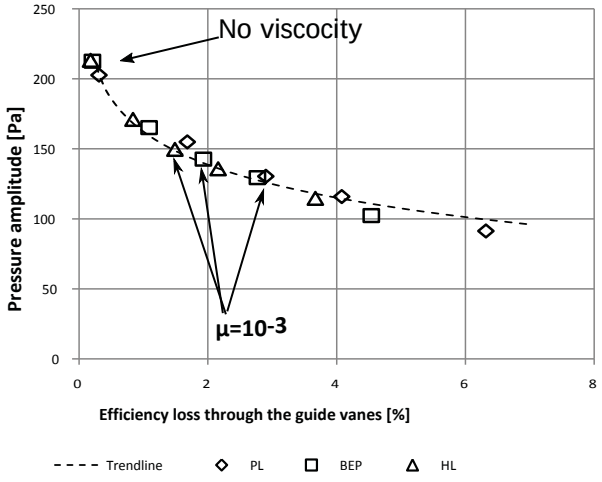

Figure 9. Average pressure amplitude in the runner vs guide vane losses

passing frequency plotted against the efficiency loss through the guide vane domain.

There are two interesting results shown in figure 9. First it shows that the pressure amplitudes can indeed be conservatively recreated using inviscous, laminar simulations. All calculated pressure amplitudes are significantly greater using the inviscid solution compared to the viscous solution. Also the trend of pressure amplitudes vs guide vane losses is very similar to the spatially varying pressure amplitudes vs guide

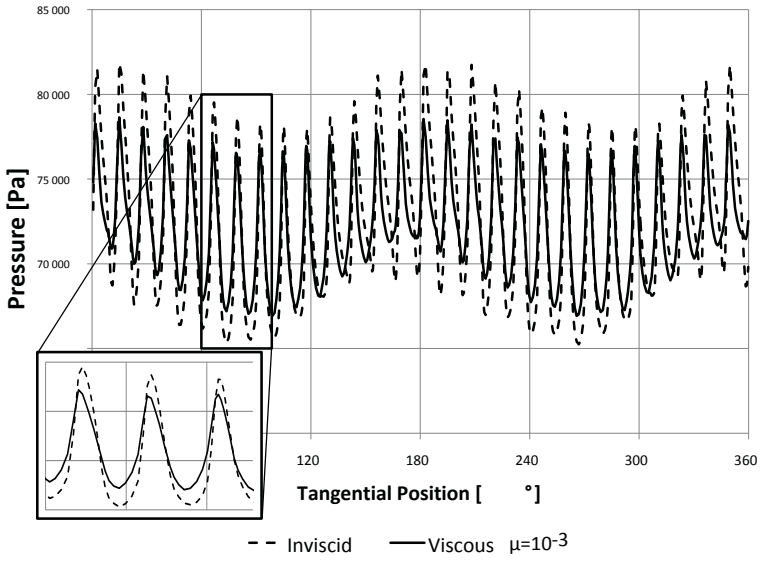

Figure 10. Instantaneous pressure field between runner and guide vanes at HL

vane loss shown in figure 5. The second interesting result from figure 9 is that changes in guide vane opening follows the same trendline as changes in viscosity . However, the increase in pressure amplitudes at greater guidevane openings is likely due to both the reduced spacing between the runner and guide vane and not only the change in friction losses and not the change in losses alone.

Another observation to be made from this is the relation between model and prototype pressure pulsations. For hydro turbines the Reynolds number is defined as in (9). When scaling a model to prototype the Reynolds number will increase. Since an increase in viscosity also is a reduction in Reynolds number, such a scaling will move the turbine left in figure 9. This means that the pressure amplitudes directly related to RSI without acoustic effects can be expected to increase slightly more than a direct scaling with head from a model test to prototype.

$$Re_u = \frac{d \cdot d \cdot \omega}{\nu} \tag{9}$$

5. Time saving

As the Euler equations have no diffusion terms and no turbulence equations, the time spent on each iteration is expected to be less than for using the Navier-Stokes equations. This is of course dependent on both the implementation of the equations in the solver and the problem at hand. Since CFX does not have a particular Euler solver, the equation solved is still the Navier-Stokes equation only with viscosity set to zero and without turbulence terms. Since slip-conditions are applied to the walls in the Euler case, the Y-plus requirements of the turbulence model is not present. However this has not been evaluated here as the mesh used is the same for both the inviscid and viscous solutions.

The calculations show that the average time spent calculating the unsteady 360° case was roughly 35% less using the laminar inviscid method compared to the turbulent viscous method. Examining on which equations the solver spends its time, it is clear that the time saved is a direct result of not solving the turbulence equations.

While a 35% reduction in time spent on each case is significant, having a pure Euler solver with a mesh tailored for the inviscid solver would most likely reduce the time even further.

6. Conclusions

Quickly producing conservative estimates for the pressure pulsations occurring inside of a low specific speed Francis turbine can be useful during a design phase. This paper has shown, both analytically and numerically, that there is a clear relation between friction losses in the guide vane cascade and the dynamic pressure variation observed in low specific speed Francis turbine calculated at the guide vane passing frequency. The observed pressure pulsations in the runner are inversly related to the friction losses.

Using conservation of momentum on a control volume around all guide vanes shows that increased friction losses have to reduce the tangential velocities which are propotional to the spatially varying pressure field squared. Observing the spatially varying pressure field behind the guide vanes from the rotating domain of the runner gives a transient pressure variation at the guide vane passing frequency. Together this shows that underestimating the friction losses, as with the inviscid Euler equations, will result in overestimation of the dynamic pressure field in the runner due to RSI.

Another observation which can be drawn from this is that pressure pulsations due to RSI increases with Reynolds number. This means that RSI-pressure pulsations observed at a modeltest will, when scaled to a prototype, increase more than a direct scaling by head.

Using the CFX solver with negligeble viscosity produced a pressure field both in the runner and in the vane less space which had similar waveforms and phase angles as the viscid solution. The pressure amplitudes were however between 50% and 100% greater compared to the fully viscid calculations. The time spent solving the inviscid flow field with out a turbulence model was found to be about 35% than the solving the viscous and turbulent flow field.

7. References

[1] Frank T. Abbott. *The effects of roughness at high Reynolds numbers on the lift and drag characteristics of three thick airfoils*. Langley Memorial Aeronautical Laboratory, 1944.
[2] Einar Agnalt. Pressure measurement inside a francis turbine runner. Master's thesis, NTNU, 2016.
[3] Øyvind Antonsen. *Unsteady flow in wicket gate and runner with focus on static and dynamic load on runner*. PhD thesis, NTNU, 2007.
[4] J. T. Billdal, Ø. Jacobsen, K. Bratsberg, H. I. Andersson, and H. Brekke. *Numerical Inviscid Flow Analysis of the GAMM Francis Runner*, pages 71–76. Vieweg+Teubner Verlag, Wiesbaden, 1993.
[5] MICHAEL B. GILES. Calculation of unsteady wake/rotor interaction. *Journal of Propulsion and Power*, 4(4):356–362, July 1988.
[6] Helmut Keck and Mirjam Sick. Thirty years of numerical flow simulation in hydraulic turbomachines. *Acta Mechanica*, 201(1):211–229, 2008.
[7] Chirag Trivedi, Michel J. Cervantes, and Ole G. Dahlhaug. Experimental and numerical studies of a high-head francis turbine: A review of the francis-99 test case. *Energies*, 9(2):74, 2016.